Extreme heat in North America, Europe and China in July 2023 made much more likely by climate change

Authors

1. Mariam Zachariah, *Grantham Institute, Imperial College London, UK*
2. Sjoukje Philip, *Royal Netherlands Meteorological Institute (KNMI), De Bilt, The Netherlands*
3. Izidine Pinto, *Royal Netherlands Meteorological Institute (KNMI), De Bilt, The Netherlands*
4. Maja Vahlberg, *Red Cross Red Crescent Climate Centre, The Hague, the Netherlands*
5. Roop Singh, *Red Cross Red Crescent Climate Centre, The Hague, the Netherlands*
6. Friederike E L Otto, *Grantham Institute, Imperial College London, UK*

Review authors

1. Clair Barnes, *Grantham Institute, Imperial College London, UK*
2. Julie Arrighi, *Red Cross Red Crescent Climate Centre, The Hague, the Netherlands*

Main findings

- Heatwaves are amongst the deadliest natural hazards with thousands of people dying from heat-related causes each year. However, the full impact of a heatwave is rarely known until weeks or months afterwards, once death certificates are collected, or scientists can analyse excess deaths. Many places lack good record-keeping of heat-related deaths, therefore currently available global mortality figures are likely an underestimate.

- In line with what has been expected from past climate projections and IPCC reports these events are not rare anymore today. North America, Europe and China have experienced heatwaves increasingly frequently over the last years as a result of warming caused by human activities, hence the current heat waves are not rare in today's climate with an event like the currently expected approximately once every 15 years in the US/Mexico region, once every 10 years in Southern Europe, and once in 5 years for China.

- Without human induced climate change these heat events would however have been extremely rare. In China it would have been about a 1 in 250 year event while maximum heat like in July 2023 would have been virtually impossible to occur in the US/Mexico region and Southern Europe if humans had not warmed the planet by burning fossil fuels.

- In all the regions a heatwave of the same likelihood as the one observed today would have been significantly cooler in a world without climate change. Similar to previous studies we found that the heatwaves defined above are 2.5°C warmer in Southern Europe, 2°C warmer in North

DOI: https://doi.org/10.25561/105549

America and about 1°C in China in today's climate than they would have been if it was not for human-induced climate change.

- Unless the world rapidly stops burning fossil fuels, these events will become even more common and the world will experience heatwaves that are even hotter and longer-lasting. A heatwave like the recent ones would occur every 2-5 years in a world that is 2°C warmer than the pre industrial climate.

- Heat action plans are increasingly being implemented across all three regions and there is evidence that they lead to reduced heat-related mortality. Furthermore, cities that have urban planning for extreme heat tend to be cooler and reduce the urban heat island effect. There is an urgent need for an accelerated roll-out of heat action plans in light of increasing vulnerability driven by the intersecting trends of climate change, population ageing, and urbanisation.

1 Introduction

Following a record hot June 2023 (Copernicus, 2023), the beginning of July 2023 saw extreme heatwaves in several parts of the Northern Hemisphere, including the Southwest of the USA and Mexico, Southern Europe, and China. Temperatures exceeded 50°C on the 16th of July in Death Valley in the USA as well as in Northwest China (CNN, 2023). Records were also reached in many other weather stations in China and the all-China heat record was broken in Sanbao on the 16th of July. The hottest night was recorded for Toksun, China. In Europe, the hottest ever day in Catalunya (Beteve, 2023) was recorded and highest ever records of daily minimum temperature were broken in other parts of Spain. On the southern side of the Mediterranean many all time records were broken in Algeria, Tunisia. In the USA parts of Nevada, Colorado and New Mexico tied their all time high, parts of Arizona, Cayman Islands, highest ever night time temperatures in Phoenix, Arizona (The Hill, 2023) which also set a record for the longest time (19 days) without falling below 90F/32.2°C.

The extreme heat affected over 100 million people across the USA alone (Reuters, 2023), where dozens of people have suffered heat-related deaths along the USA-Mexico border and throughout Arizona (CNN, 2023; Axios, 2023; The New York Times, 2023; ABC, 2023; Wola, 2023). An additional 211 fatalities have been reported in Mexico, nearly half of whom in the state of Nuevo León (El Mercurio, 2023; Tribuna de Mexico, 2023), along with at least four people in Italy, all while undertaking construction work (Independent, 2023; AMP Today, 2023; La Repubblica, 2023; Leggo, 2023), three in China (South China Morning Post, 2023; PBS, 2023), and one in Spain, Cyprus, and Algeria, respectively (Yeni Safak, 2023; Phys, 2023; La Nouvelle République, 2023). Several thousands of cases of heat-related illness have moreover been reported across North America (El Sol de Zacatecas, 2023; Reuters, 2023), Europe, notably in Italy, Greece, Cyprus, Spain, and North Macedonia (Phys, 2023; CNN, 2023; LBC, 2023; Sky News, 2023; AP News, 2023, TIME, 2023), North Africa, notably in Algeria (La Nouvelle République, 2023), and eastern China (PBS, 2023, China Daily, 2023; AP News, 2023). In northern Syria, the extreme heat is particularly hard-hitting to internally displaced persons residing in camps, as temperatures are significantly exacerbated in tents and energy poverty has left people without reliable access to active cooling such as fans (Al Jazeera, 2023). In line with robust scientific evidence on the differential vulnerability to extreme heat (see e.g. Benmarhnia et al., 2015; Arsad et al., 2022), the elderly, young children, outdoor workers, and people living in homelessness and

DOI: https://doi.org/10.25561/105549

displacement are disproportionately affected by the high temperatures currently scorching the Northern Hemisphere.

Beyond its effects on human health, the heatwave has also led to record-breaking power demand increases across China (CNN, 2023) as well as power outages, mainly in the USA and Europe (Los Angeles Times, 2023; The Washington Post, 2023). Large-scale crop damage and livestock losses have been reported throughout all affected regions, including for corn and soybeans in the USA (NBC News, 2023), coffee, maize, beans, oats, and sugarcane, and the death of at least 200 cattle in Mexico (TV Azteca, 2023; La Prensa Latina, 2023), projected drops in the olive harvest in Spain, Italy, and Portugal (The Guardian, 2023), productivity losses in milk production and tomato crop damage in Italy (NBC News, 2023; The Guardian, 2023), and reductions in grain harvest and cotton production in China (South China Morning Post, 2023; Caixin Global, 2023). The heat is moreover aggravating pre-existing water stress in Morocco, the USA, Turkey, and Iran (Newsweek, 2023; NPR, 2023; Iran Wire, 2023; RFI, 2023). Low water levels of European rivers, including the Rhine, are also limiting shipping as barges must carry less (Gulf News, 2023), and risks restricting power output of two nuclear power plants in France that use water to cool reactors (Reuters, 2023). Due to prolonged high temperatures and dry conditions, wildfires are raging cross western USA (The Washington Post, 2023; AP News, 2023), Puerto Rico (CNN, 2023), Spain, notably the Canary Islands (The Guardian, 2023; Sky News, 2023), Greece (BBC, 2023; Reuters, 2023; Independent, 2023), Switzerland (Barrons, 2023), Croatia (KFGO, 2023), and Turkey (AP News, 2023), displacing thousands of people and causing hazardous spikes in air pollution. These impacts are threatening agriculture-dominant economies and food and water security, and increasing food prices (see e.g. RFI, 2023; South China Morning Post, 2023), leading to further devastating knock-on effects on domestic and global scales.

In this study, we investigate the role of human-induced climate change in the likelihood and intensity of these extreme heatwaves in three distinct regions. To achieve this, we follow the established methods of multi-model multi-method approach of extreme event attribution (Philip et al., 2020; van Oldenborgh et al., 2021). This approach has been used in many case studies on extreme heat events, including the Mediterranean (Philip et al., 2023), North America (Philip et al., 2021), Siberia (Ciavarella et al., 2020), Western Europe (Vautard et al., 2019), India and Pakistan (Zachariah et al., 2022), Argentina (Rivera et al., 2022), and South Asia (Zachariah et al., 2023).

To capture the events leading to the impacts described above we focus on three regions: the Southwestern USA and Northern Mexico, Southern Europe, and the low-lands of China. Figure 1 shows the maximum temperatures over the hottest periods in July and the anomalies with respect to the 1950-2022 average of daily maximum temperatures in the peak summer months of July and August.

We focus the analysis on the maximum temperatures in the global regions where anomalously high temperatures have been reported during the on-going summer season, and many people have been affected by the heat: North America (Texas, California, Arizona, New Mexico and Nevada in the USA, Baja California, Sonora, Chihuahua, and Coahuila in Mexico); Southern Europe (Spain, Italy, Greece and the Balkan states neighbouring the Mediterranean); and China. While the extreme heat was an important driver of the observed impacts, it is important to highlight that the meteorological extremes assessed here only partly represent one component of these described impacts, which also strongly depend on exposure and vulnerability, as well as other climatological components of the meteorological hazard. In addition we highlight that the Southern USA as well as Southern Europe has been suffering from recurrent drought conditions, likely worsening the heat. Although high nighttime temperatures - which are associated with severely increased risks to health - have also been recorded, many of the

DOI: https://doi.org/10.25561/105549

immediate reported impacts have been due to record daytime temperatures, therefore we focus on daily maximum temperatures here.

In this study, we define the event using three distinct definitions, with each definition specifically tailored to one of the three regions under investigation, shown in Figure 1:

1. USA/Mexico: annual maxima of 18-day mean of daily maximum temperatures (Tx18day) over the most affected regions in western USA, Texas and northern Mexico.
2. Southern Europe: annual maxima of 7-day mean of daily maximum temperatures (Tx7day) over land cells in the rectangular box 5W-25E, 36-45N.
3. China: annual maxima of 14-day mean of daily maximum temperatures (Tx14day), over the lowlands in China.

In each case, spatial and temporal averaging are carried out before finding the time series of annual maxima.

DOI: https://doi.org/10.25561/105549

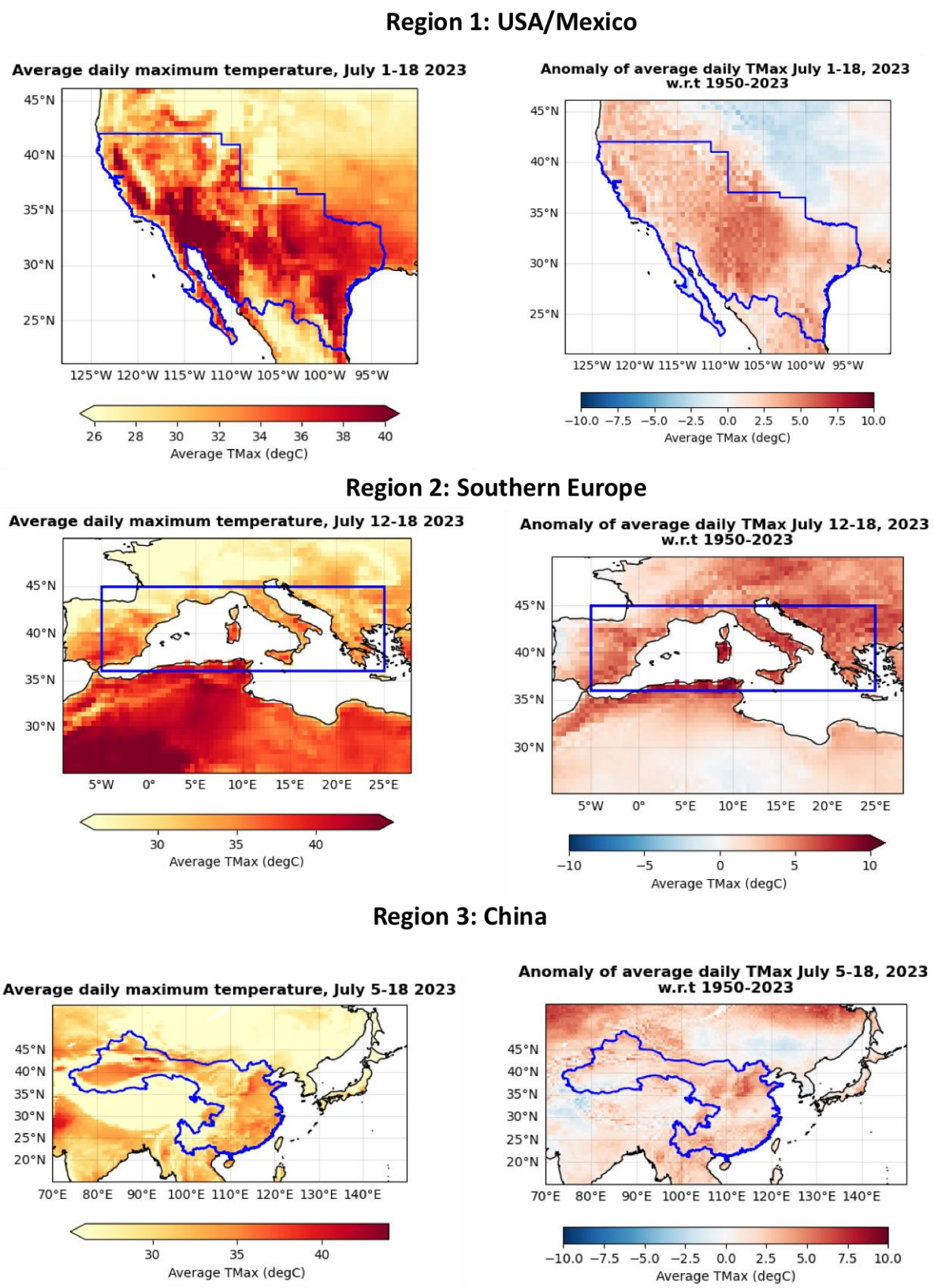

Figure 1: Maximum July temperatures averaged over the length of the heat events defined for this study (left-hand side) and the same but expressed in anomalies with respect to 1950-2023 (right-hand side). The first row shows the Western USA and Mexico, the second Southern Europe and the third row China.

DOI: https://doi.org/10.25561/105549

Due to the particularly short time frame in which it was produced, this document presents a more limited analysis than other World Weather Attribution studies. The analysis follows the peer-reviewed World Weather Attribution Protocol (Philip et al, 2020) but unlike most studies, only one reanalysis dataset is used in the observational analysis, and one multi-model ensemble in the attribution. Furthermore, preliminary reanalysis data have been used in the observational analysis. This may have an influence on the estimated return period, although based on past experience in similar studies the effect on the overall result is likely to be small. For more details on differences in the methods see Section 2.3.

The AR6 WGI report stresses that Mediterranean regions have in general already undergone increases in heat waves and agro-ecological droughts, attributable to climate change with respectively high and medium confidence (Summary for Policy Makers, Figure 3). Warming of between 0.2°C and 0.3°C per decade has been observed in the Central America region, reaching 0.5°C per decade in Mexico and southern Baja California in the last 30 years (Gutiérrez et al, 2021). In the Asian continent, there has been a clear and substantial warming of temperatures over the past century. Additionally, extreme heat episodes have noticeably increased in frequency across most regions of the continent (Seneviratne et al, 2021). In a warming scenario, it is very likely that trends in hot extremes will continue to intensify (IPCC, 2021). The current heatwaves are therefore among the many consequences expected from climate change, and this is reflected in the fact that none of the events assessed in this study have been found to be particularly rare in the current climate.

2 Data and methods

2.1 Observational data

We use the daily maximum temperatures (Tmax) over the three defined regions from the European Centre for Medium-Range Weather Forecasts (ECMWF) ERA5 reanalysis product (Hersbach et al., 2020). It should be noted that the variables from ERA5 are not directly assimilated, but these are generated by atmospheric components of the Integrated Forecast System (IFS) modelling system. The reanalysis begins in 1950, with data available until the end of the preceding month (June 2023). We extend the reanalysis data with the preliminary ECMWF analysis (1-16 July) and the ECMWF forecast (17-23 July) to cover the period of the three events. This is preliminary data but this is unlikely to affect the conclusions of the analysis.

As a measure of anthropogenic climate change we use the (low-pass filtered) global mean surface temperature (GMST) taken from the National Aeronautics and Space Administration (NASA) Goddard Institute for Space Science (GISS) surface temperature analysis (GISTEMP, Hansen et al., 2010 and Lenssen et al. 2019).

2.2 Model and experiment descriptions

In this super-rapid analysis, we follow the approach used in the previous super-rapid study on extreme heat in the western Mediterranean region and use only one multi-model ensemble, CMIP6 (Eyring et al., (2016)). For this study we analysed a set of 19 models of the CMIP6 ensemble with varying resolutions. For all simulations, the period 1850 to 2015 is based on historical simulations, while the SSP5-8.5 scenario is used for the remainder of the 21st century. Each CMIP6 model has its own land-

DOI: https://doi.org/10.25561/105549

sea mask and this is used to select land-only grid cells in the study area for this analysis, keeping the native resolution of each model. Only one ensemble member from each model is analysed for each region. Each model's own GMST is used as covariate, smoothed with a 4-year running mean.

2.3 Statistical methods

We analyse time series of the three event definitions (see section 1): i) Tx18day over the western US, Texas and northern Mexico region, ii) Tx7day over the Southern European rectangular box (5W-25E, 36-45N), and iii) Tx14day over the lowlands of China. Methods for observational and model analysis and for model evaluation and synthesis are used according to the World Weather Attribution Protocol, described in Philip et al. (2020), with supporting details found in van Oldenborgh et al. (2021), Ciavarella et al. (2021) and here.

The analysis steps include: (i) trend calculation from observations; (ii) model validation; (iii) multi-method multi-model attribution and (iv) synthesis of the attribution statement.
We calculate the return periods, Probability Ratio (PR; the factor-change in the event's probability) and change in intensity of the event under study in order to compare the climate of now and the climate of the past, defined respectively by the GMST values of now and of the preindustrial past (1850-1900, based on the Global Warming Index). To statistically model the event under study, we use a Generalised Extreme Value (GEV) distribution that shifts with GMST. Next, results from the ERA5 reanalysis and the individual CMIP6 models that pass the evaluation tests are synthesised into a single attribution statement.

There are some small differences between the model evaluation method used in this super-rapid analysis and a standard WWA analysis following the protocol. The model evaluation step here assesses the seasonal cycle and statistical fit parameters, but not the spatial pattern of the temperatures, which are known to be relatively well represented at these large scales. Models with large temperature biases (ie. for which a 1-in-N-year event was particularly hot or cool) were also excluded; a sensitivity analysis was carried out in which the synthesis was repeated both including and excluding these models, and the overall results were not strongly affected.

3 Observational analysis: return period and trend

High temperatures and heat waves are usually recorded in the months of July and August in all three study regions. Figure 2 shows the time series of annual maxima of N-day average daily maximum temperature (TxNday) in the three study regions - USA/Mexico (left), South Europe (middle) and China (right). In the USA/Mexico region, Tx18day is higher in 2023 than all years since 1950, breaking records for daily maximum temperatures despite occurring at the beginning of the heatwave season. The 2023 7-day temperatures in Southern Europe, although not the highest observed, are still very high with only marginally higher temperatures (by ~0.2C and ~0.4C) experienced in 2017 and 2021. Over lowland China, the 2023 14-day event, although extreme, is not the highest observed, with higher temperatures in 1953, 1956, 2015-17 and 2022. However, this is largely due to the selection of the study region, and the temporal definition adopted in this study for this event: these were intended to cover all the impacted regions in China, from Xinjiang province in the west to Beijing in the east, and at slightly different times during the ongoing heatwave season. However, a clear increase in N-day daily maximum

DOI: https://doi.org/10.25561/105549

temperatures is evident in all of these cases, being higher in USA/Mexico and Southern Europe regions than in China.

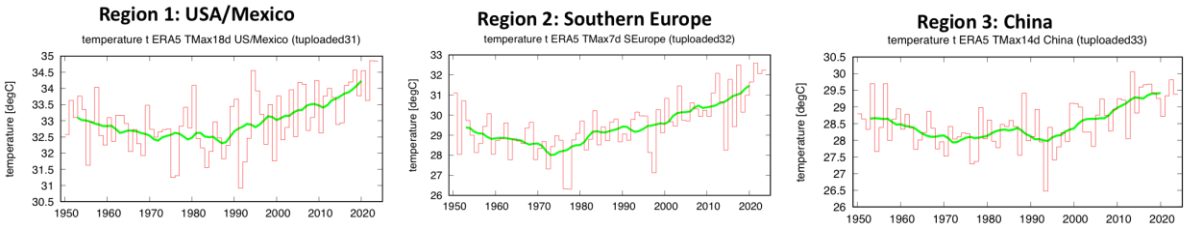

Figure 2: *Time series of annual maxima of 18-day average daily maximum temperature along with the ten-year running mean (shown by green line) for US/Mexico region* ***(left).*** *Same as (left) for the 7-day average for Southern Europe region (**middle**). Same as (left) for the 14-day average for lowlands of China (**right**).*

The left-hand panels in Figure 3 show the fitted trend in TxNday in ERA5 for the three study regions against observed GMST anomalies. The temperatures show relatively stronger response to GMST in the USA/Mexico and Southern Europe domains than over lowland China: Tx18day events in the USA/Mexico region (top left) estimated to be 1.6°C hotter (uncertainty: 1.0-2.1°C) in the 2023 climate than in a preindustrial climate; Tx7day in Southern Europe are 2.9°C hotter (uncertainty: 2.0-3.9°C, middle left); and Tx14day in lowland China 1.1°C hotter (uncertainty: 0.6-1.6°C, bottom left).

The right-hand panels of Figure 3 show estimated return period curves for the 2023 climate and a 1.2°C cooler climate. The return period of the 2023 event in the current climate is 13 years (uncertainty 7-53 years) for the USA/Mexico region (top right); for South Europe, the 2023 event has a return period of 9 years (uncertainty: 5-32 years; middle right); and in lowland China, 3 years (uncertainty 2-6 years; bottom right). For the attribution analysis, we use return periods of 15 years for the USA/Mexico event, 10 years for South Europe, and 5 years for China.

Probability ratios (PRs) reflect the estimated factor change in probability of exceeding the observed temperatures due to a 1.2°C increase in GMST: that is, how many times more likely it is that TxNday will exceed the observed temperatures in each region, due to the increase in GMST from preindustrial levels to the 2023 climate. The best estimate for PR tends to infinity for the USA/Mexico and Southern European domains, with lower bounds of 950 and 4400 respectively. For China, the PR is 33 (uncertainty: 5 to infinity).

DOI: https://doi.org/10.25561/105549

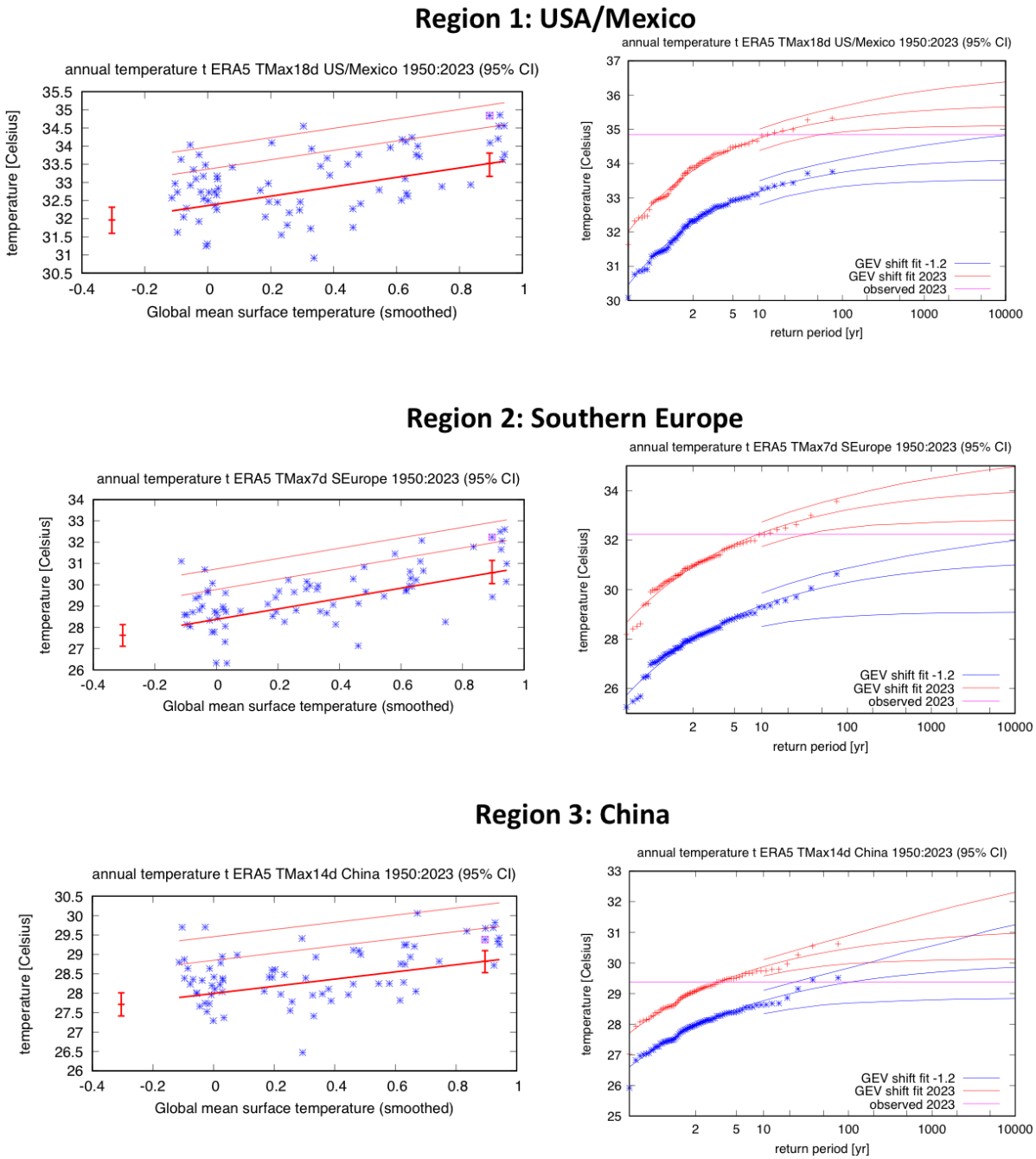

Figure 3: (Left-hand panels) *Linear trend in ERA5 TxNday as a function of GMST. The thick red line denotes the location parameter of the fitted distribution, and the thin red lines show 6-year and 40-year return levels. The vertical red lines show the 95% confidence interval for the location parameter, for the 2023 climate and a hypothetical 1.2ºC cooler climate. The 2023 observation is highlighted with the magenta box.* ***(Right-hand panels)*** *GEV-based return periods for TxNday at 2023 GMST (red lines) and a 1.2ºC cooler GMST (blue lines with 95% CI). Lines above and below the main trend represent 95% confidence intervals obtained via a bootstrapping procedure.*

4 Model evaluation

There are some small differences between the model evaluation method used in this super-rapid analysis and a standard WWA analysis. Here, we do not assess how well the individual climate models capture the seasonal cycle or spatial pattern of the temperatures, which are known to be relatively well

DOI: https://doi.org/10.25561/105549

represented at these large scales. Climate models are evaluated against the observations in their ability to capture the observed distribution of TxNday, and discarded if the ranges of the scale and shape parameters of the fitted nonstationary GEV do not overlap with those estimated from ERA5. The models are labelled as 'good', 'reasonable', or 'bad' for each parameter. Models with large temperature biases (ie. for which a 1-in-N-year event was particularly hot) were also marked as 'reasonable' rather than 'good'; a sensitivity analysis was carried out in which the synthesis was repeated both including and excluding these models, and the overall results were not strongly affected.
If the model is 'good' for all criteria, we give it an overall rating of 'good'. We rate the model as 'reasonable' or 'bad', if it is rated 'reasonable' or 'bad', respectively, for at least one criterion. In the tables below we show the results of the model validation for the three study regions. In each case, if more than five models achieve a 'good' evaluation overall, then only these models are included in the attribution; if five models or fewer achieve this, then models deemed 'reasonable' are also included.

Table 1**:** *Evaluation results of the climate models considered for attribution analysis of Tx18day over the USA/Mexico domain. For each model, the expected temperature of a 1-in-15-year event is shown, along with the best estimate of the scale and shape parameters and a 95% confidence interval for each, obtained via bootstrapping. The qualitative evaluation is shown in the right-hand column.*

Model / Observations	**Observed 2023 (°C)**	**Scale parameter**	**Shape parameter**	**Conclusion**
ERA5	34.84	0.786 (0.655 ... 0.900)	-0.35 (-0.50 ... -0.20)	
	Temperature of 1-in-15 year event			
ACCESS-CM2 historical-ssp585 (1)	35.83	0.770 (0.530 ... 0.910)	-0.46 (-0.65 ... -0.22)	good
ACCESS-ESM1-5 historical-ssp585 (1)	36.61	0.810 (0.580 ... 0.950)	-0.12 (-0.34 ... 0.10)	reasonable
CanESM5 historical-ssp585 (1)	39.27	0.620 (0.420 ... 0.740)	-0.040 (-0.18 ... 0.16)	bad
CMCC-ESM2 historical-ssp585 (1)	36.85	0.860 (0.560 ... 1.03)	-0.35 (-0.55 ... -0.070)	good
EC-Earth3 historical-ssp585 (1)	36.85	0.860 (0.560 ... 1.03)	-0.35 (-0.55 ... -0.070)	reasonable (not used due to issues with execution)
EC-Earth3-Veg historical-ssp585 (1)	36.85	0.860 (0.560 ... 1.03)	-0.35 (-0.55 ... -0.070)	reasonable (not used due to issues with execution)
EC-Earth3-Veg-LR historical-ssp585 (1)	37.01	0.960 (0.660 ... 1.13)	-0.35 (-0.51 ... -0.080)	reasonable
FGOALS-g3 historical-ssp585 (1)	35.15	0.920 (0.700 ... 1.07)	-0.20 (-0.39 ... 0.010)	reasonable
INM-CM4-8 historical-ssp585 (1)	38.9	1.03 (0.750 ... 1.21)	-0.30 (-0.67 ... -0.15)	reasonable
INM-CM5-0 historical-ssp585 (1)	38.72	1.46 (0.920 ... 1.78)	-0.44 (-0.70 ... -0.22)	bad
MIROC6 historical-ssp585 (1)	47.83	1.08 (0.720 ... 1.29)	-0.39 (-0.62 ... -0.17)	reasonable, very high threshold

DOI: https://doi.org/10.25561/105549

MPI-ESM1-2-HR historical-ssp585 (1)	36.86	0.770 (0.520 ... 0.940)	-0.35 (-0.63 ... -0.10)	good
MPI-ESM1-2-LR historical-ssp585 (1)	36.91	0.840 (0.650 ... 0.950)	-0.35 (-0.65 ... -0.18)	good
MRI-ESM2-0 historical-ssp585 (1)	38.89	1.11 (0.830 ... 1.27)	-0.27 (-0.46 ... -0.090)	reasonable
NorESM2-MM historical-ssp585 (1)	37.32	0.720 (0.540 ... 0.840)	-0.37 (-0.56 ... -0.17)	good
TaiESM1 historical-ssp585 (1)	38.04	0.870 (0.680 ... 1.00)	-0.14 (-0.36 ... 0.030)	reasonable

Table 2**:** *Evaluation results of the climate models considered for attribution analysis of Tx7day over the Southern Europe domain. For each model, the expected temperature of a 1-in-10-year event is shown, along with the best estimate of the scale and shape parameters and a 95% confidence interval for each, obtained via bootstrapping. The qualitative evaluation is shown in the right-hand column.*

Model / Observations	Observed 2023 (**°C**)	**Sigma**	**Shape parameter**	**Conclusion**
ERA5	32.23	1.04 (0.808 ... 1.20)	-0.29 (-0.53 ... -0.17)	
	Temperature of 1-in-10 year event			
ACCESS-CM2 historical-ssp585 (1)	34.4	1.09 (0.810 ... 1.25)	-0.12 (-0.45 ... 0.10)	reasonable
ACCESS-ESM1-5 historical-ssp585 (1)	36.81	1.43 (1.10 ... 1.68)	-0.36 (-0.56 ... -0.14)	reasonable
CanESM5 historical-ssp585 (1)	35.46	1.28 (0.880 ... 1.52)	-0.39 (-0.55 ... -0.11)	reasonable
CMCC-ESM2 historical-ssp585 (1)	36.92	1.43 (1.07 ... 1.63)	-0.26 (-0.59 ... -0.10)	reasonable
CNRM-CM6-1-HR historical-ssp585 (1)	32.17	1.43 (1.12 ... 1.62)	-0.25 (-0.45 ... -0.050)	reasonable
CNRM-CM6-1 historical-ssp585 (1)	31.69	1.27 (0.890 ... 1.54)	-0.39 (-0.56 ... -0.19)	reasonable
EC-Earth3 historical-ssp585 (1)	36.1	1.14 (0.830 ... 1.35)	-0.13 (-0.27 ... 0.060)	reasonable
EC-Earth3-Veg historical-ssp585 (1)	37.15	1.22 (0.820 ... 1.47)	-0.25 (-0.50 ... 0.060)	reasonable (not used due to issues with execution)
EC-Earth3-Veg-LR historical-ssp585 (1)	36.49	1.26 (0.980 ... 1.46)	-0.21 (-0.39 ... -0.050)	reasonable (not used due to issues with execution)
FGOALS-g3 historical-ssp585 (1)	36.49	1.26 (0.980 ... 1.46)	-0.21 (-0.39 ... -0.050)	reasonable
INM-CM4-8 historical-ssp585 (1)	44.05	1.24 (0.840 ... 1.48)	-0.44 (-0.75 ... -0.28)	reasonable, very high threshold
INM-CM5-0 historical-ssp585 (1)	42.98	1.21 (0.970 ... 1.37)	-0.35 (-0.57 ... -0.14)	reasonable, very high threshold

DOI: https://doi.org/10.25561/105549

IPSL-CM6A-LR historical-ssp585 (1)	31.06	1.10 (0.810 ... 1.29)	-0.25 (-0.46 ... 0.0)	good
MIROC6 historical-ssp585 (1)	42.97	1.11 (0.780 ... 1.31)	-0.090 (-0.30 ... 0.15)	reasonable, very high threshold
MPI-ESM1-2-HR historical-ssp585 (1)	35.38	1.48 (1.07 ... 1.72)	-0.20 (-0.34 ... -0.030)	reasonable
MPI-ESM1-2-LR historical-ssp585 (1)	36.57	1.37 (0.960 ... 1.64)	-0.32 (-0.50 ... -0.10)	reasonable
MRI-ESM2-0 historical-ssp585 (1)	32.26	1.48 (1.16 ... 1.71)	-0.43 (-0.69 ... -0.25)	reasonable, only just within uncertainty
NorESM2-MM historical-ssp585 (1)	35.28	1.11 (0.840 ... 1.27)	-0.13 (-0.29 ... 0.030)	reasonable
TaiESM1 historical-ssp585 (1)	38.35	1.50 (0.970 ... 1.80)	-0.24 (-0.41 ... 0.010)	reasonable, very high threshold

Table 3**:** *Evaluation results of the climate models considered for attribution analysis of Tx14day over the lowland China domain. For each model, the expected temperature of a 1-in-5-year event is shown, along with the best estimate of the scale and shape parameters and a 95% confidence interval for each, obtained via bootstrapping. The qualitative evaluation is shown in the right-hand column.*

Model / Observations	Observed 2023 (°C)	**Sigma**	**Shape parameter**	**Conclusion**
ERA5	29.384	0.622 (0.460 ... 0.743)	-0.26 (-0.44 ... -0.070)	
	Temperature of 1-in-5 year event			
ACCESS-CM2 historical-ssp585 (1)	30.57	0.610 (0.440 ... 0.710)	-0.18 (-0.33 ... 0.020)	good
ACCESS-ESM1-5 historical-ssp585 (1)	30.76	0.710 (0.510 ... 0.830)	-0.22 (-0.44 ... 0.030)	good
CanESM5 historical-ssp585 (1)	31.97	0.570 (0.430 ... 0.660)	-0.12 (-0.31 ... 0.070)	good
CMCC-ESM2 historical-ssp585 (1)	30.87	0.520 (0.400 ... 0.600)	-0.090 (-0.36 ... 0.12)	good
EC-Earth3 historical-ssp585 (1)	30.87	0.520 (0.400 ... 0.600)	-0.090 (-0.36 ... 0.12)	good
EC-Earth3-Veg historical-ssp585 (1)	30.87	0.520 (0.400 ... 0.600)	-0.090 (-0.36 ... 0.12)	good
EC-Earth3-Veg-LR historical-ssp585 (1)	29.4	0.780 (0.520 ... 0.900)	-0.17 (-0.41 ... 0.010)	reasonable (not used due to issues with execution)
FGOALS-g3 historical-ssp585 (1)	33.19	0.690 (0.540 ... 0.770)	-0.30 (-0.52 ... -0.080)	reasonable (not used due to issues with execution)
INM-CM4-8 historical-ssp585 (1)	29.83	0.490 (0.310 ... 0.580)	-0.19 (-0.34 ... 0.070)	reasonable
INM-CM5-0 historical-ssp585 (1)	29.73	0.610 (0.460 ... 0.720)	-0.23 (-0.67 ... 0.0)	good

DOI: https://doi.org/10.25561/105549

MIROC6 historical-ssp585 (1)	36.16	0.680 (0.520 ... 0.810)	-0.10 (-0.32 ... 0.070)	good
MPI-ESM1-2-HR historical-ssp585 (1)	31.07	0.690 (0.520 ... 0.780)	-0.23 (-0.49 ... -0.080)	good
MPI-ESM1-2-LR historical-ssp585 (1)	29.95	0.620 (0.470 ... 0.710)	-0.29 (-0.52 ... -0.030)	good
MRI-ESM2-0 historical-ssp585 (1)	32.71	0.530 (0.400 ... 0.610)	-0.070 (-0.33 ... 0.11)	good
NorESM2-MM historical-ssp585 (1)	32.07	0.700 (0.550 ... 0.810)	-0.23 (-0.54 ... -0.080)	good
TaiESM1 historical-ssp585 (1)	31.86	0.550 (0.370 ... 0.650)	-0.19 (-0.42 ... 0.060)	

5 Multi-model attribution

This section shows Probability Ratios (PRs) and change in intensity ΔI for ERA5 and the CMIP5 models that passed evaluation for each region

5.1 USA/Mexico

	a. Past vs. present		b. Present vs. future	
Model / Observations	**Probability ratio PR [-]**	**Change in intensity ΔI [˚C]**	**Probability ratio PR [-]**	**Change in intensity ΔI [˚C]**
ERA5	∞ (9.5e+2 ... ∞)	1.6 (1.0 ... 2.1)		
ACCESS-CM2 historical-ssp585 (1)	1.0e+4 (1.0e+4 ... 1.0e+4)	1.6 (1.1 ... 2.2)	4.9 (3.8 ... 16)	1.1 (0.94 ... 1.3)
ACCESS-ESM1-5 historical-ssp585 (1)	19 (1.8 ... 1.0e+4)	1.8 (1.2 ... 2.4)	5.1 (4.0 ... 10)	1.0 (0.87 ... 1.2)
CMCC-ESM2 historical-ssp585 (1)	1.0e+4 (52 ... 1.0e+4)	2.1 (1.6 ... 2.5)	6.3 (4.8 ... 14)	1.2 (0.99 ... 1.4)
EC-Earth3-Veg-LR historical-ssp585 (1)	1.0e+4 (26 ... 1.0e+4)	2.0 (1.5 ... 2.4)	7.7 (5.7 ... 17)	1.3 (1.1 ... 1.4)
FGOALS-g3 historical-ssp585 (1)	91 (7.1 ... 1.0e+4)	1.1 (0.69 ... 1.6)	3.7 (2.9 ... 6.7)	0.72 (0.54 ... 0.90)
INM-CM4-8 historical-ssp585 (1)	1.0e+4 (19 ... 1.0e+4)	1.8 (1.1 ... 2.5)	5.8 (4.4 ... 18)	1.3 (1.1 ... 1.6)

DOI: https://doi.org/10.25561/105549

MIROC6 historical-ssp585 (1)	1.0e+4 (1.0e+4 ... 1.0e+4)	2.5 (1.6 ... 3.4)	6.5 (5.1 ... 12)	1.6 (1.3 ... 1.9)
MPI-ESM1-2-HR historical-ssp585 (1)	1.0e+4 (6.9 ... 1.0e+4)	1.5 (0.98 ... 2.2)	6.3 (4.7 ... 22)	1.1 (0.85 ... 1.3)
MPI-ESM1-2-LR historical-ssp585 (1)	1.0e+4 (∞ ... 1.0e+4)	2.0 (1.3 ... 2.6)	7.4 (5.6 ... 22)	1.3 (1.1 ... 1.5)
MRI-ESM2-0 historical-ssp585 (1)	1.0e+4 (76 ... 1.0e+4)	1.9 (1.1 ... 2.6)	4.9 (3.9 ... 13)	1.3 (1.1 ... 1.6)
NorESM2-MM historical-ssp585 (1)	1.0e+4 (4.8e+3 ... 1.0e+4)	2.2 (1.6 ... 2.9)	9.5 (7.0 ... 36)	1.4 (1.3 ... 1.6)
TaiESM1 historical-ssp585 (1)	4.3e+2 (19 ... 1.0e+4)	1.9 (1.3 ... 2.4)	5.8 (4.5 ... 10)	1.1 (0.96 ... 1.2)

5.2 Southern Europe

	a. Past vs. present		b. Present vs. future	
Model / Observations	**Probability ratio PR [-]**	**Change in intensity ΔI [˚C]**	**Probability ratio PR [-]**	**Change in intensity ΔI [˚C]**
ERA5	∞ (4.4e+3 ... ∞)	2.9 (2.1 ... 3.9)		
ACCESS-CM2 historical-ssp585 (1)	1.5e+2 (20 ... ∞)	2.0 (1.3 ... 2.7)	4.0 (3.3 ... 6.1)	1.5 (1.2 ... 1.7)
ACCESS-ESM1-5 historical-ssp585 (1)	1.0e+4 (1.0e+4 ... ∞)	2.7 (2.0 ... 3.4)	6.0 (4.7 ... 9.8)	2.1 (1.8 ... 2.3)
CanESM5 historical-ssp585 (1)	2.6e+3 (46 ... ∞)	3.1 (2.5 ... 3.9)	4.0 (3.4 ... 6.1)	1.7 (1.5 ... 2.0)
CMCC-ESM2 historical-ssp585 (1)	1.0e+4 (30 ... ∞)	2.5 (1.5 ... 3.4)	4.7 (3.9 ... 11)	1.7 (1.4 ... 2.0)
CNRM-CM6-1-HR historical-ssp585 (1)	77 (10 ... ∞)	2.0 (1.3 ... 2.7)	3.9 (3.2 ... 5.7)	1.6 (1.3 ... 1.9)
CNRM-CM6-1 historical-ssp585 (1)	58 (11 ... ∞)	1.7 (1.0 ... 2.4)	3.9 (3.2 ... 6.2)	1.5 (1.3 ... 1.8)
EC-Earth3 historical-ssp585 (1)	12 (4.9 ... ∞)	1.4 (0.76 ... 1.9)	3.8 (3.3 ... 5.7)	1.4 (1.2 ... 1.6)

DOI: https://doi.org/10.25561/105549

EC-Earth3-Veg historical-ssp585 (1)	1.0e+4 (73 ... ∞)	2.4 (1.8 ... 2.9)	4.3 (3.5 ... 6.3)	1.4 (1.2 ... 1.6)
EC-Earth3-Veg-LR historical-ssp585 (1)	5.1e+2 (29 ... ∞)	2.4 (1.5 ... 3.2)	4.8 (3.9 ... 7.8)	1.8 (1.5 ... 2.0)
INM-CM4-8 historical-ssp585 (1)	1.0e+4 (1.0e+4 ... ∞)	2.3 (1.7 ... 3.1)	5.9 (4.5 ... 24)	1.7 (1.3 ... 1.9)
INM-CM5-0 historical-ssp585 (1)	1.0e+4 (1.0e+4 ... ∞)	2.8 (2.0 ... 3.6)	6.6 (4.9 ... 15)	1.8 (1.6 ... 2.0)
IPSL-CM6A-LR historical-ssp585 (1)	1.6e+2 (6.1 ... ∞)	1.7 (0.94 ... 2.3)	5.3 (4.2 ... 7.6)	1.6 (1.4 ... 1.7)
MIROC6 historical-ssp585 (1)	4.7e+2 (5.4 ... ∞)	2.4 (0.76 ... 3.8)	5.5 (4.3 ... 8.1)	2.4 (1.8 ... 2.8)
MPI-ESM1-2-HR historical-ssp585 (1)	1.5e+2 (11 ... ∞)	2.0 (1.1 ... 3.0)	4.0 (3.3 ... 6.1)	1.5 (1.2 ... 1.8)
MPI-ESM1-2-LR historical-ssp585 (1)	1.0e+4 (1.0e+4 ... ∞)	2.7 (2.1 ... 3.4)	5.9 (4.4 ... 14)	2.2 (1.9 ... 2.6)
MRI-ESM2-0 historical-ssp585 (1)	1.0e+4 (63 ... ∞)	2.3 (1.5 ... 3.3)	4.1 (3.4 ... 6.0)	1.5 (1.2 ... 1.7)
NorESM2-MM historical-ssp585 (1)	2.5e+4 (49 ... ∞)	2.6 (1.9 ... 3.5)	6.8 (5.3 ... 13)	2.1 (1.9 ... 2.4)
TaiESM1 historical-ssp585 (1)	6.9e+3 (51 ... ∞)	2.7 (1.8 ... 3.7)	4.0 (3.3 ... 5.6)	1.6 (1.4 ... 1.8)

5.3 China

	a. Past vs. present		b. Present vs. future	
Model / Observations	**Probability ratio PR [-]**	**Change in intensity ΔI [˚C]**	**Probability ratio PR [-]**	**Change in intensity ΔI [˚C]**
ERA5	32.6 (5.02 … ∞)	1.11 (0.595, 1.61)		
ACCESS-CM2 historical-ssp585 (1)	1.0e+4 (3.5e+2 ... 1.0e+4)	1.9 (1.5 ... 2.2)	4.1 (3.2 ... 5.6)	1.2 (1.1 ... 1.4)
ACCESS-ESM1-5 historical-ssp585 (1)	1.0e+4 (6.7e+2 ... 1.0e+4)	1.5 (1.1 ... 1.9)	4.0 (3.1 ... 5.3)	1.3 (1.2 ... 1.4)

DOI: https://doi.org/10.25561/105549

CanESM5 historical-ssp585 (1)	11 (5.4 ... 2.1e+2)	0.98 (0.70 ... 1.2)	3.3 (2.8 ... 4.3)	0.95 (0.85 ... 1.1)
CMCC-ESM2 historical-ssp585 (1)	43 (13 ... 9.9e+2)	1.5 (1.1 ... 1.8)	3.6 (3.0 ... 4.5)	0.98 (0.84 ... 1.1)
EC-Earth3-Veg-LR historical-ssp585 (1)	1.1 (0.53 ... 2.3)	0.070 (-0.39 ... 0.57)	2.0 (1.6 ... 2.4)	0.52 (0.33 ... 0.68)
FGOALS-g3 historical-ssp585 (1)	5.2e+2 (30 ... 1.0e+4)	1.3 (0.97 ... 1.6)	3.6 (2.9 ... 4.7)	0.94 (0.80 ... 1.1)
INM-CM4-8 historical-ssp585 (1)	14 (5.2 ... 6.2e+3)	1.1 (0.73 ... 1.4)	3.6 (3.0 ... 5.0)	0.90 (0.76 ... 1.1)
INM-CM5-0 historical-ssp585 (1)	2.6e+2 (28 ... 1.0e+4)	1.2 (0.86 ... 1.6)	3.7 (3.1 ... 5.1)	0.90 (0.78 ... 1.0)
MIROC6 historical-ssp585 (1)	1.5 (0.40 ... 5.1)	0.22 (-0.52 ... 0.93)	2.7 (2.3 ... 3.3)	0.84 (0.63 ... 1.1)
MPI-ESM1-2-HR historical-ssp585 (1)	76 (12 ... 1.0e+4)	1.0 (0.54 ... 1.4)	3.3 (2.8 ... 5.4)	1.0 (0.74 ... 1.2)
MPI-ESM1-2-LR historical-ssp585 (1)	79 (13 ... 1.0e+4)	1.3 (0.90 ... 1.7)	3.7 (3.0 ... 4.8)	1.2 (0.97 ... 1.4)
MRI-ESM2-0 historical-ssp585 (1)	1.0e+4 (77 ... 1.0e+4)	1.6 (0.92 ... 2.1)	3.8 (3.1 ... 5.3)	1.2 (1.0 ... 1.3)
NorESM2-MM historical-ssp585 (1)	67 (9.5 ... 1.0e+4)	1.5 (0.92 ... 2.1)	4.0 (3.2 ... 5.3)	1.3 (1.1 ... 1.4)
TaiESM1 historical-ssp585 (1)	1.0e+4 (1.5e+2 ... 1.0e+4)	1.8 (1.4 ... 2.1)	3.9 (3.2 ... 5.2)	1.1 (0.99 ... 1.2)

6 Hazard synthesis

For the event definitions described in Section 1 we evaluate the influence of anthropogenic climate change by calculating the probability ratio as well as the change in intensity using observations and climate models. Models which do not pass the validation tests described in Section 4 are excluded from the analysis.

The aim of this step in the assessment is to synthesise results from models that pass the evaluation along with the observation-based products, to give an overarching attribution statement. In this study however, for two out of the three regions - the USA/Mexico region and Southern Europe - the probability ratio is infinite for the observations and about half the models used in this analysis. Therefore, a numerical synthesis of the change in probability is essentially meaningless, because finite results can only be obtained by replacing infinity with an arbitrary finite number. The numerical synthesis can therefore

DOI: https://doi.org/10.25561/105549

only give a lower bound, which is highly uncertain. What we can say with certainty is that the temperatures experienced in these two regions would have been extremely unlikely to have occurred without human induced climate change. In contrast, the change in intensity is well-bounded and much less uncertain. We therefore only report a numerical synthesis for the changes in intensity in all three regions.

Figures 4-6 show the changes in probability and intensity in all three regions for the observations (blue) and models (red). To combine them into a synthesised assessment, a term to account for intermodel spread is added in quadrature to the natural variability of the models. This is shown in the figures as white boxes around the light red bars. The dark red bar shows the model average, consisting of a weighted mean using the uncorrelated uncertainties due to natural variability plus the term representing intermodel spread (ie, the inverse square of the white bars). Observation-based products and models are combined into a single result in two ways. Firstly, we neglect common model uncertainties beyond the intermodel spread that is depicted by the model average, and compute the weighted average of models (dark red bar) and observations (dark blue bar): this is indicated by the magenta bar. Because, due to common model uncertainties, model uncertainty can be larger than the intermodel spread, secondly, we also show the more conservative estimate of an unweighted, direct average of observations (dark red bar) and models (dark blue bar) contributing 50% each, indicated by the white box around the magenta bar in the synthesis figures.

We repeat the same assessment for simulations of a 0.8°C warmer future from today, i.e. a 2°C warmer world compared to a preindustrial climate. Because no observations exist for the future, only model results are shown.

As noted above, the probability ratios are highly dependent on how the infinity values are dealt with in the numerical assessment, thus the only conclusion that we can draw with very high confidence is that they are very large. Climate change made these events several orders of magnitude more likely in North America and Europe. We can thus conclude that without climate change these events would have been virtually impossible to occur or, given the lower bounds seen in the upper left panels of Figures 4-5, they have been made at least 1000 more likely. For China, the change is slightly smaller, with an increase in probability of 52.7 (3.54 to 4110) which we round to about 50 times more likely.

In a 0.8°C warmer world the events will become even more frequent with an additional increase in likelihood of a factor 2 or higher, rendering the return times of these events to approximately once every 2 to 5 years.

In all the regions a heatwave of the likelihood observed today would have been significantly cooler in a world without climate change. In the Southern Europe region, the change in intensity combining observations and model is 2.5°C (2.0 to 3.2). It is important to highlight however, that the observations show a larger increase, of up to 4°C. In a 0.8°C warmer future a heat event like this would be another 1.7°C hotter (1.2 to 2.2).

For the other two regions changes in intensity are smaller, with 1.78°C increase (1.38 to 2.01) up to today for the North American Region and a further increase of 1.18°C in a 2°C world (0.85 to 1.50) and 1.19°C increase up to today in China (0.29 to 2.09) and a further increase of 1.02°C in a 2°C world (0.63 to 1.41).

DOI: https://doi.org/10.25561/105549

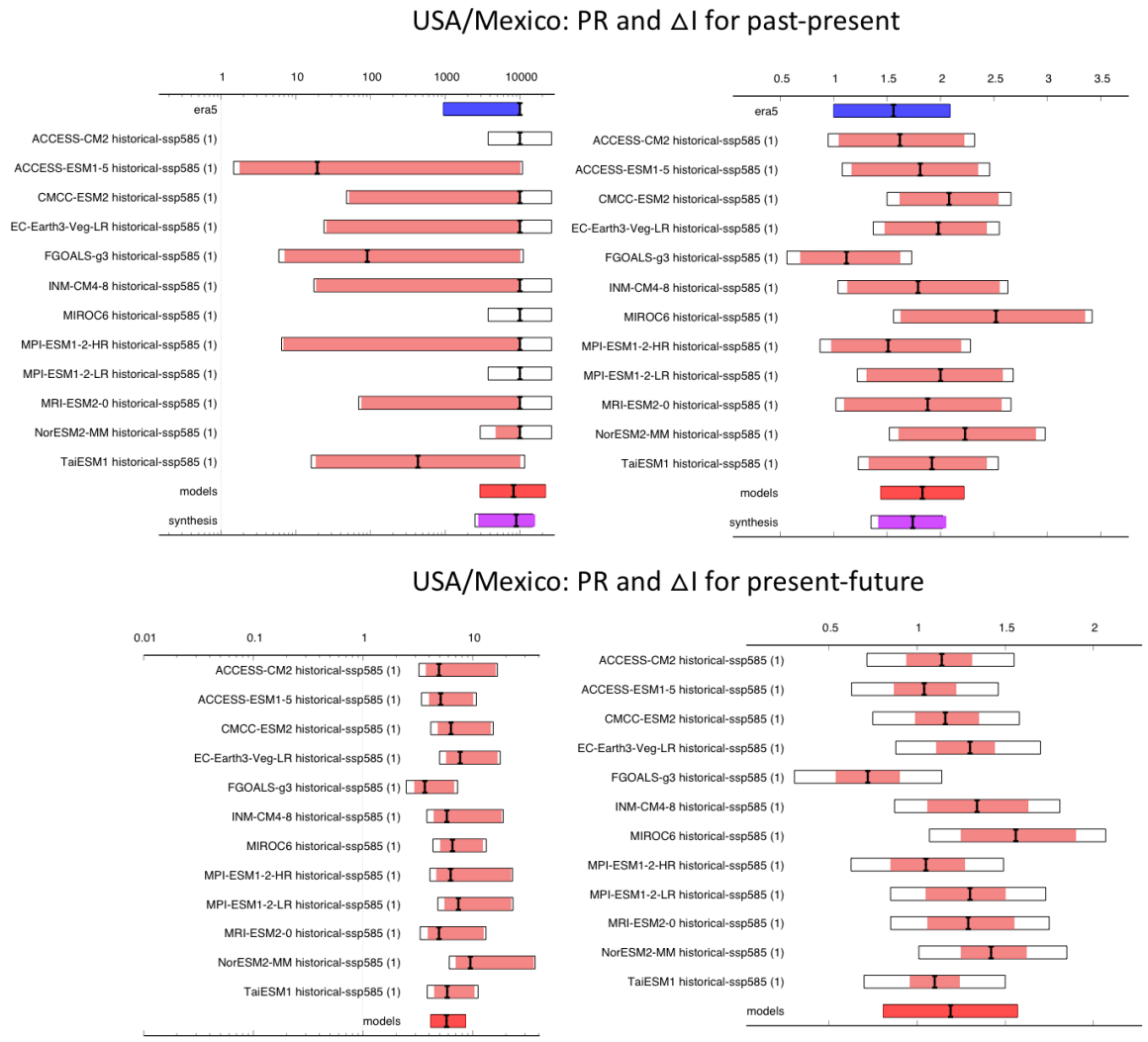

Figure 4: *Synthesis of (left) probability ratios and (right) intensity changes when comparing the return period and magnitudes of Tx18day in the USA/Mexico region: (top) between the current climate and a 1.2°C cooler climate and (bottom) between the current climate and a 0.8°C warmer climate (ie. with total warming of 2°C). Infinite probability ratios are truncated at 10000.*

DOI: https://doi.org/10.25561/105549

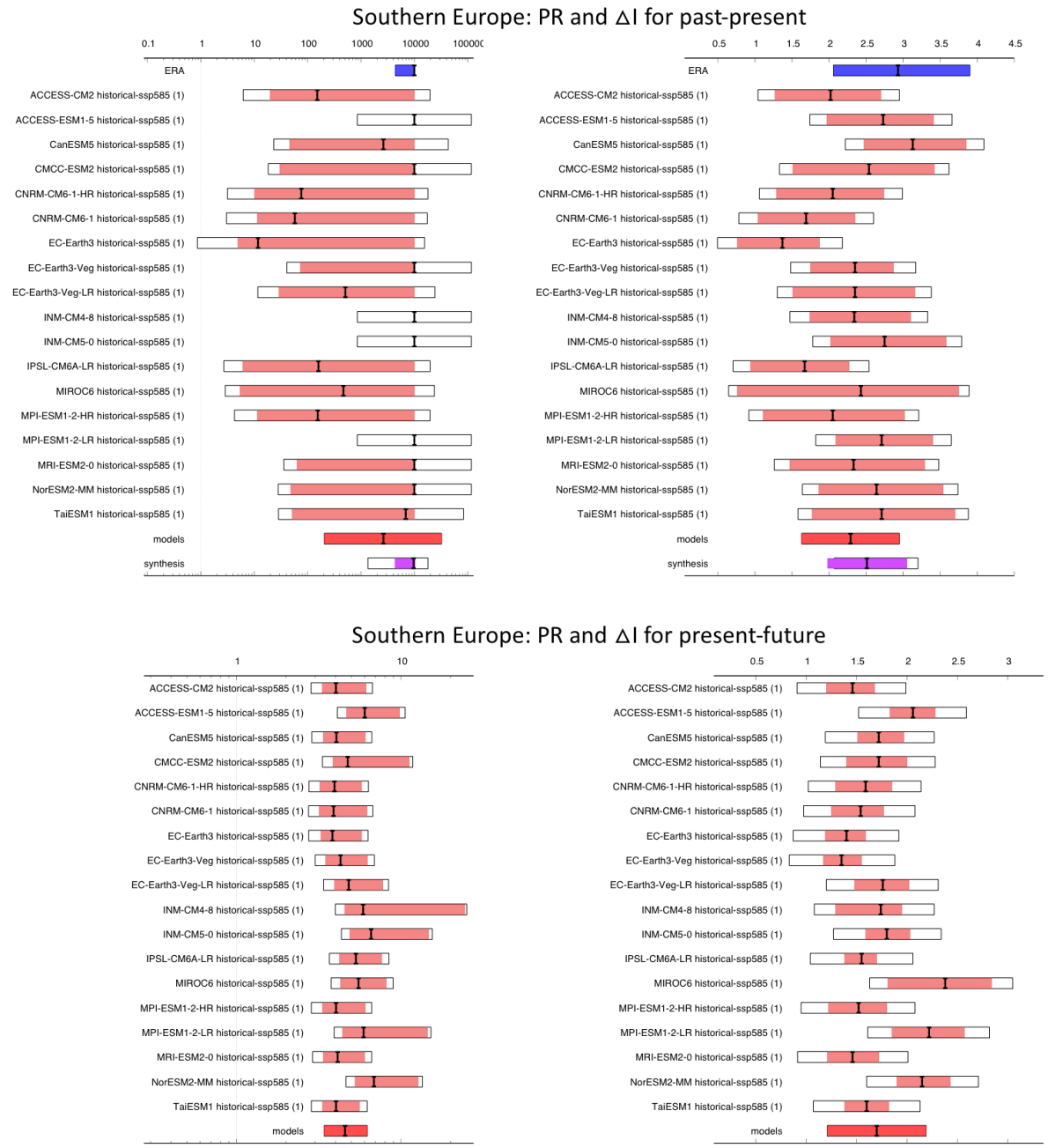

Figure 5: *Synthesis of (left) probability ratios and (right) intensity changes when comparing the return period and magnitudes of Tx7day in the Southern Europe region: (top) between the current climate and a 1.2°C cooler climate and (bottom) between the current climate and a 0.8°C warmer climate (ie. with total warming of 2°C). Infinite probability ratios are truncated at 10000.*

DOI: https://doi.org/10.25561/105549

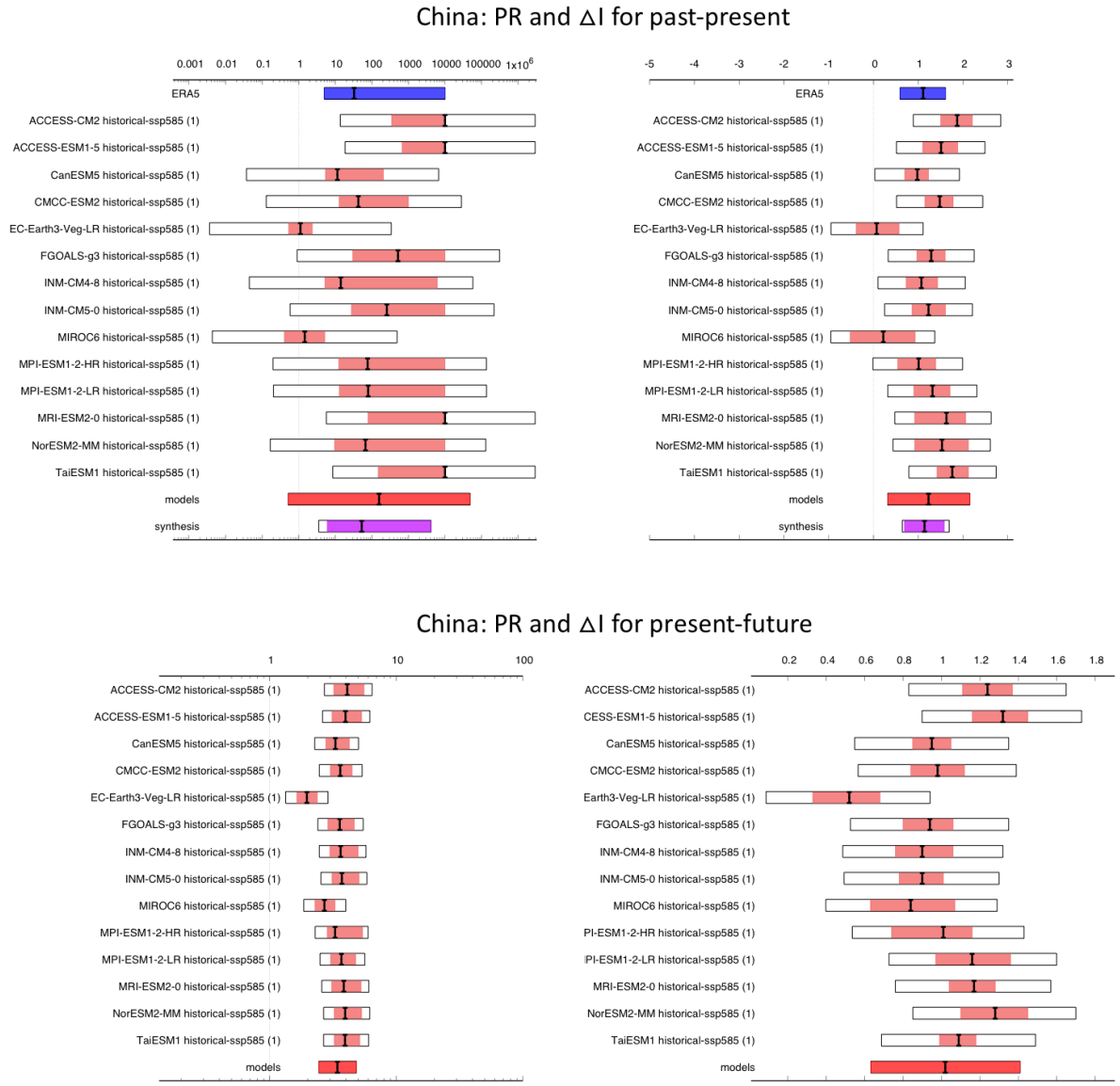

Figure 6: *Synthesis of (left) probability ratios and (right) intensity changes when comparing the return period and magnitudes of Tx14day in the lowland China region: (top) between the current climate and a 1.2°C cooler climate and (bottom) between the current climate and a 0.8°C warmer climate (ie. with total warming of 2°C). Infinite probability ratios are truncated at 10000.*

DOI: https://doi.org/10.25561/105549

7 Vulnerability and exposure

Heatwaves are amongst the deadliest natural hazards with thousands of people dying from heat-related causes each year (EM-DAT). However, the full impact of a heatwave is often not known until weeks or months afterwards, once death certificates are collected, or scientists can analyse excess deaths. In many cases, we never know the full extent of the impact to human health because heat-related deaths are often attributed to other causes like kidney failure or cardiac arrest, when they would not have occurred had the high temperatures not exacerbated someone's pre-existing condition, or they are not counted at all. Despite this, we have observed instances such as the 2022 Europe heat season with at least 61,000 deaths (Ballester et al., 2023), in addition to the 2010 Russian and 2021 North American heatwaves with over 55,000 and 1,000 deaths, respectively (CRED, 2011; Keith and Meerow, 2022). The correlation between extreme heat and increases in mortality has been well established by research, in Europe and North Africa (Rodrigues et al., 2021; Royé et al., 2020; Ahmadalipour and Moradkhani, 2018), North America (Shindell et al., 2021; Sheridan et al., 2021; Fever et al., 2022), China (Luo et al., 2019; Yang et al., 2021), and globally (Green et al., 2019, Mora et al., 2017, Calleja-Agius, England & Calleja, 2022).

To date, hundreds of heat-related fatalities have been reported across the studied regions, of which 211 have occurred in Mexico (El Mercurio, 2023). However, heatwaves do not need to result in excess deaths. Simple actions like checking in on your neighbours, drinking enough water, and finding a cool place to go during the hottest part of the day can save lives if instituted systematically by governments through heat action plans (Singh et al., 2019). As of 2022, 17 out of the European Union's 53 member states had developed national heat health action plans (HHAPs) since the deadly 2003 heatwave that took over 70,000 lives (Sanchez Martinez et al., 2022; Robine et al., 2008). Among the 17 HHAPs, several core elements (as outlined by the WHO guidelines) remain gaps, notably reduction in indoor heat exposure, long-term urban planning, and real-time surveillance and evaluation (Sanchez Martinez et al., 2022). While trends of climate change, population ageing, and urbanisation are exacerbating vulnerability (see e.g. Harrington and Otto, 2023), many parts of Europe and North America are experiencing decreases in heat-related health impacts (Sanchez Martinez et al., 2022; Hasan et al., 2021; Benmarhnia et al., 2019). This suggests that heat action implemented to date is indeed helping strengthen resilience.

Further measures that can help save lives include ensuring the availability of active cooling devices such as air conditioners and fans, and the ability of electrical grids to cope with an increase in demand. Across several urban centres in eastern China, the power consumption has surged and broken records (CNN, 2023). Despite this, power outages remain limited (Baijahao Baidu, 2023; South China Morning Post, 2023). The long list of measures implemented by the State Grid Corporation of China to ensure reliable access to energy in Beijing include having increased staffing by 9,300 people, deployed 165 emergency power generation vehicles on standby, and opened a 24-hour emergency power transmission service to ensure availability for people to purchase energy (Baijahao Baidu, 2023). Research on heat mortality in Beijing confirms the positive role of active cooling as a coping mechanism when faced with extreme heat (Yin & Wang, 2017; Xing et al., 2020). While this was likely life-saving, it should be mentioned that significant upscaling to coal production and burning was key to meeting this demand. Shanghai was, for instance, reported to be burning 800 tons of coal per hour to help its 26 million inhabitants withstand the heat (Bloomberg, 2023).

DOI: https://doi.org/10.25561/105549

Similarly, it is crucial that health services are prepared to deal with an influx of heat patients. In Italy, hospitals report an up to 25% heat-related increase in admissions (La Repubblica, 2023), urging regional governments to activate a "heat code" to establish fast-track access to emergency rooms for patients suffering from heat strokes (The Guardian, 2023). Similar protocols have been activated in Greece (Greek Reporter, 2023).

Due to urban heat island (UHI) effects, cities experience notably higher temperatures compared to their rural surroundings (Copernicus, n.d.). In Athens (Greece), and Miami-Dade, Phoenix, and Los Angeles (US), four of the world's currently eight Chief Heat Officers (CHOs) are mandated by their respective cities to coordinate heat action for increased resilience among vulnerable inhabitants. This includes updating the Climate Action Plan and supporting the development of a green and blue infrastructure city project across Athens (Atlantic Council, n.d.), creating a multi-stakeholder Climate and Heat Health Task Force in Miami-Dade (Miami-Dade County, n.d.), developing an action plan to reduce heat-related mortality and hospitalizations in Los Angeles (Department of Public Works, 2022), and establishing an heat action plan to address the increasing urban heat risks in Phoenix (City of Phoenix, 2021). To prevent impacts during this period of relentless heat, all four cities, and many more, opened cooling centres to provide relief for vulnerable city dwellers (CBS News, 2023; The Guardian, 2023; The Washington Post, 2023; Ekathimerini, 2023). In Athens, the Acropolis was closed for tourists (Sky News, 2023), work during afternoons was suspended in high risk areas and workers with health issues within the private sector requested to work remotely (NBC News, 2023), and public and private sector services underwent changes to their operating hours to limit unnecessary travel during the hottest hours of the day (Greek Reporter, 2023). In Nuevo León in northern Mexico, one of the worst-affected states in terms of heat mortality to date, over 96% of the population resides in urban centres (Atlantic Council, 2022). The state capital, Monterrey, had a CHO between April 2022 and April 2023; the Officer was an architect specialised in urban planning, making her well-placed to advance the mainstreaming of passive cooling design, which has shown promising results to reduce indoor heat in pilot programs throughout low-income neighbourhoods (Gladu, 2022). In Europe, much of the existing building stock was built before modern-day thermal standards and results in an increased demand for active cooling during heatwaves (EEA, 2023). Retrofitting and designing new infrastructure with passive cooling strategies (e.g. passive solar shade, insulation, natural ventilation, building orientation and shape) can help to reduce energy demand and costs (EEA, 2023).

Cities that have urban planning for extreme heat tend to be cooler and reduce the urban heat island effect. Research by Marando et al. (2022) on the ecosystem services of green areas in over 600 European cities shows that vegetation-based spaces cool urban centres by up to 2.9°C and 1.07°C on average. On average across the studied cities, to reduce urban temperatures by 1, 2 or 3°C, a city needs a 16%, 32%, or 48% tree cover, respectively (Marando et al., 2022). Similarly, Colunga et al. (2015) suggest that the UHI effect in the central Mexican city of Querétaro could drop by 2.05°C if the urban zone canopy cover would increase by 50%.

Data availability

All data are available via the Climate Explorer.

DOI: https://doi.org/10.25561/105549

References

All references are given as hyperlinks in the text.

Please cite this report as:

Zachariah, M; Philip, S; Pinto, I; Vahlberg, M; Singh, R; Arrighi, J; R; Barnes, C; Otto, FEL (2023). Extreme heat in North America, Europe and China in July 2023 made much more likely by climate change.

DOI: https://doi.org/10.25561/105549